Proceedings of the 39th IAHR World Congress
19-24 June 2022
Granada, Spain
DOI number

Validation of a Dual-tip Conductivity Probe by a High-speed Stereo-camera Setup for Air-water Flow Properties Estimation

Simone Pagliara[1], Benjamin Hohermuth[2] and Robert M. Boes[3]

[1,2,3] Laboratory of Hydraulics, Hydrology and Glaciology (VAW), ETH Zurich, Zurich, Switzerland
e-mail pagliara@vaw.baug.ethz.ch

Abstract

High-velocity air-water flows are frequently observed at hydraulic structures, e.g., spillways and low-level outlets, and they are characterized by a strong interaction between the two phases and by void fractions ranging from a few percent to up to 100% at the free surface. Intrusive phase-detection probes represent the most widely used instrumentation in hydraulic engineering to measure air-water flow properties, such as void fraction, interfacial velocity, and particle chord lengths. Such probes are especially effective for applications characterized by high levels of aeration where optical and acoustic techniques would fail. Herein, an experimental setup capable of producing air bubbles moving vertically at selected velocities is presented. The setup consists of (i) a vertical, acrylic glass pipe with variable water flow rates, (ii) an air-injection system with variable air flow rates, and (iii) a stereo-camera setup, comprising a beam splitter and a high-speed camera. The beam splitter setup allows simultaneously obtaining perpendicular stereo images of the bubbles, enabling three-dimensional information on bubble velocities and shape to be recorded. The bubble properties reconstructed from the high-speed images were compared to interfacial velocities and chord times obtained from a dual-tip phase-detection conductivity probe. In conclusion, the results from this study help to quantify the measurement uncertainty of commonly used air-water flow instrumentation. The details on the three-dimensional features of the bubbles may also enable to further improve the design of phase-detection probes in future studies.

Keywords: Air-water flow properties; Air bubbles; Dual-tip phase-detection probe; Conductivity probe; Image processing.

1. INTRODUCTION

Gas-liquid flows play an important role in both natural environments, e.g., mountain streams and breaking waves as well as in industrial applications, e.g., nuclear reactors and chemical plants (Tian et al., 2015) and water infrastructure. Many investigations aiming at enhancing the knowledge of two-phase flows were performed in the past, including studies on void fraction and flow patterns (e.g., Kaichiro & Ishii, 1984; Xing et al., 2014), and interfacial area concentration (Shen et al., 2006; Lucas et al., 2011; Shen et al., 2012). In the past decades, different measurement techniques have been developed and used to obtain the main local interfacial parameters, i.e., interfacial velocity, void fraction, and interfacial area concentration (Hibiki et al., 1998; Shen et al., 2005; Chanson, 2013). These include non-intrusive techniques such as video imaging, laser Doppler anemometry (LDA), particle image velocimetry (PIV), and intrusive techniques, e.g., multi-sensor electrical and optical probes. The formers are applicable only to flows characterized by low void fractions to avoid interference of bubbles with the optical or acoustic signal, thus limiting their applicability in the context of many hydraulic engineering problems including highly turbulent air-water flows occurring in dam spillways and low-level outlets (Felder & Pfister, 2017; Kramer & Chanson, 2019; Felder et al., 2019, Kramer et al., 2020a). At the same time, phase-detection intrusive probes have been used for many decades as a reliable instrument for investigating air-water flow properties and for providing key design guidelines (e.g., Boes and Hager, 2003; Pfister et al., 2014). In this regard, a wide range of intrusive phase detection probe systems characterized by different tip diameters, spacing, acquisition and data analyses methods were developed at various laboratories, e.g., Institut de mécanique de Grenoble (Cartellier & Achard, 1991), University of Queensland (see Chanson and Toombes, 2002), Nihon University (see Takahashi and Ohtsu, 2012), RWTH Aachen University (see Felder and Chanson, 2014), and UNSW Australia (see Felder and Severi, 2016). The use of such probes to study two-phase flows covered a wide range of applications in hydraulics, e.g., stepped spillway flows (Boes and Hager, 2003), hydraulic jumps (Chanson, 2007), water jets (Neto et al.,2008), cavitation phenomena (Barre et al., 2009), chute aeration (Kramer & Hager, 2005), as well as in other areas, e.g., nuclear engineering (Ishii & Kim, 2001), processing engineering (Nguyen & Bui, 2019), and chemical engineering (Wongwailikhit et al., 2019).

©2022 IAHR. Used with permission / ISSN-L 2521-7119

Intrusiveness indeed represents the major intrinsic limitation of phase-detection probes, and many studies highlighted the main biases affecting measured velocities in highly aerated flows; these include (a) biases due to particle-probe interaction (Vejražka et al., 2010), (b) biases due to the non-alignment of the probe sensors with the streamlines of the water flow (Wang et al., 2021), and (c) biases due to multiple particles impacting the probe at high velocities (Kramer et al., 2020b). The effects of intrusiveness of dual-tip probes were also documented by many studies which focused on videos from high-speed cameras, showing a strong crawling effect during the bubble-probe interaction, i.e., bubble deformations and deceleration (Vejražka et al., 2010; Perret, 2016). In the process of a bubble interacting with a dual-tip probe, three stages are clearly distinguished (Hohermuth et al., 2021): (i) prior to interaction, when the undisturbed flow surrounds the leading tip (Fig. 1a, b); (ii) during the leading tip piercing, which includes bubble deformation and crawling effect (Fig. 1c); and (iii) during the combined piercing of the leading and trailing tip, characterized by enhanced crawling effect (Fig. 1d, e, f).

In this paper, the velocities and chord times of air bubbles rising in vertically upwards pipe flow at different water velocities were measured with a dual-tip conductivity probe, and then compared to measurements made from videos recorded by a high-speed camera. Finally, the present work aims at analyzing the major sources of error characterizing dual-tip phase-detection conductivity probe.

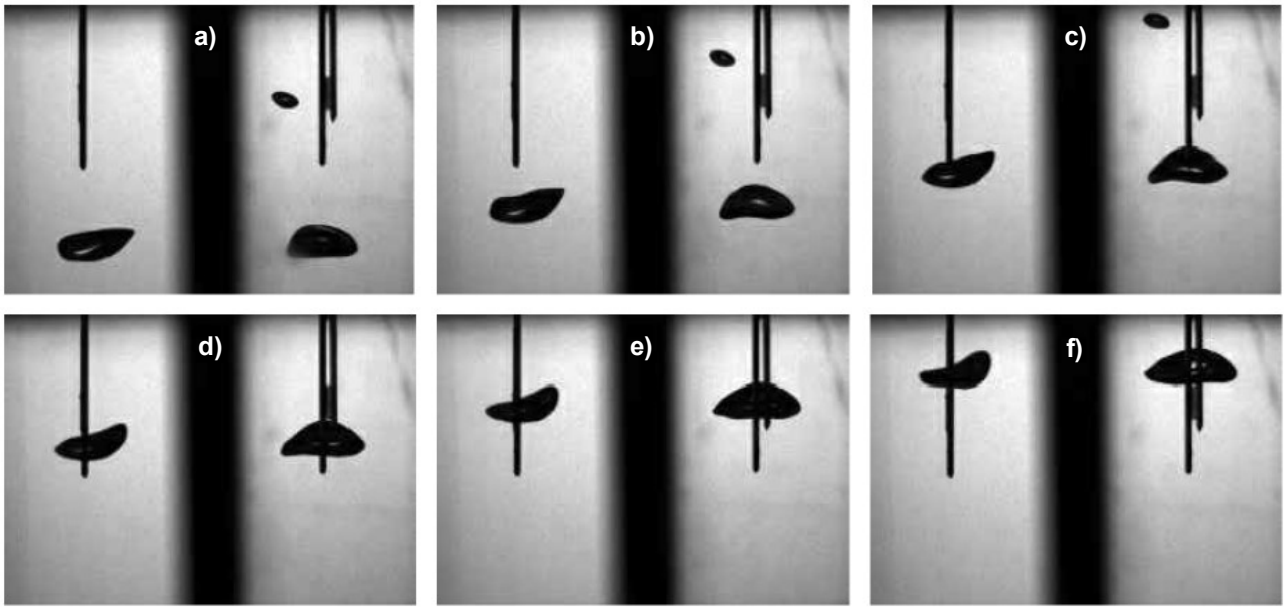

Figure 1. Interaction between a rising bubble and the tips of the phase-detection probe at different stages, (a,b) before, (c,d) during, (e,f) after interaction (Test n. 3-1, water velocity = 1 m/s, bubble diameter = 5 mm).

2. EXPERIMENTAL SETUP

An experimental setup allowing the observation of single air bubbles impacting a dual-tip conductivity probe surrounded by a rising, vertical water flow was built in the Laboratory of Hydraulics, Hydrology and Glaciology (VAW) at ETH Zurich. The setup consisted of a pressurized-flow circuit characterized by variable water discharge (Fig. 2). An acrylic-glass pipe with a length of 1.5 m, an inner diameter of 0.09 m and a wall thickness of 0.005 m was installed vertically. Water was taken from a distribution pipe and conveyed to the vertical pipe by means of steel pipes with an inner diameter of 0.08 m. The water flow was controlled by a gate valve and the flow discharge was measured by a E+H Promag 50 electromagnetic flow meter. Air bubbles were inserted from the bottom end of the vertical pipe via a narrow, L-shaped capillary steel tube connected to a butterfly valve, a pressure reduction valve and an air compression system. In the upper portion of the test pipe, a dual-tip conductivity probe was installed in a way that the tips were aligned with the central axis of the pipe, facing downwards. A U-shaped recirculation pipe collected the water flow from the top cross-section of the acrylic-glass pipe and conveyed it to the underground recirculation channel. Finally, a custom-made beam splitter and a high-speed camera were placed at the height of the probe tips, allowing a synchronized stereo-view of the rising bubbles impacting the probe. To avoid distortion effects, two flat acrylic-glass windows forming a 90° angle between them were installed on the vertical pipe (see Fig. 4).

©2022 IAHR. Used with permission / ISSN-L 2521-7119

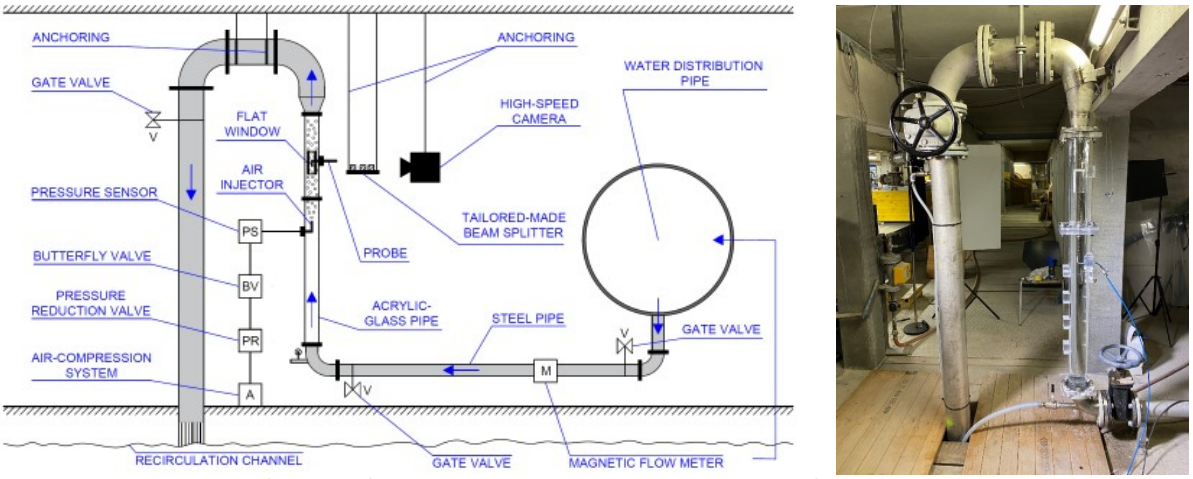

Figure 2. Sketch of the experimental setup and picture of the main structure.

2.1 Dual-tip Conductivity Probe

A dual-tip conductivity phase-detection probe previously used at VAW (e.g., Hohermuth et al., 2021) was tested in the experimental setup described. This was manufactured at the UNSW Water Research Laboratory (WRL), and it had a similar design to many probes used in past years to investigate the properties of air-water flows (e.g., Toombes & Chanson, 2008; Felder & Chanson, 2017). The probe was characterized by sensors composed of an inner electrode of diameter Φ = 0.125 mm made of platinum wire, and an outer electrode of diameter Φ = 0.600 mm made of hypodermic needles. The sensors were located side-by-side, displaced Δy = 3.94 mm in the streamwise direction, Δz = 0.97 mm in transverse and roughly aligned in the vertical direction, i.e., Δx = 0 mm (see Fig. 7). The conductivity probe raw signal was amplified with a WRL electronic unit to a range of 0 to 4.5 V and it was sampled by means of a high-speed data acquisition unit (NIUSB-6366) controlled with a LabVIEW environment. Pictures of the dual-tip probe used in the present study can be found in Felder et al., 2019.

2.2 Air Bubbles Injection

Compressed air was injected into the rising water flow through a nozzle inserted into a special block installed on the acrylic-glass vertical pipe, roughly 0.8 m downstream of the probe. The nozzle was made of a steel rod drilled along its central axis, with an external diameter of 6 mm and an internal diameter of 3 mm. On its upper extremity, a thread made it possible to screw in special elements allowing to vary the inner diameter d_n (Fig. 3). For the experimental campaign described here, the nozzle diameter was set to d_n = 1 mm. The L-shape of the nozzle helped to reduce turbulence and disturbance at the point of bubble injection. The nozzle was connected by FESTO air tubes (Φ = 4 mm) to a Keller PAA26 pressure sensor with 1 mbar accuracy, measuring the pressure P_a of the injected air. The air flow was controlled by a custom-made manual butterfly valve and a FESTO M5 pneumatic pressure reduction valve with output pressures ranging 0.5 – 7 bar, connected to a compressed air system at 10 bar. The setup resulted in the injection of bubbles with an equivalent diameter ranging between 2.5 < d_{eq} < 6.5 mm, i.e., the diameter of a sphere of equal volume.

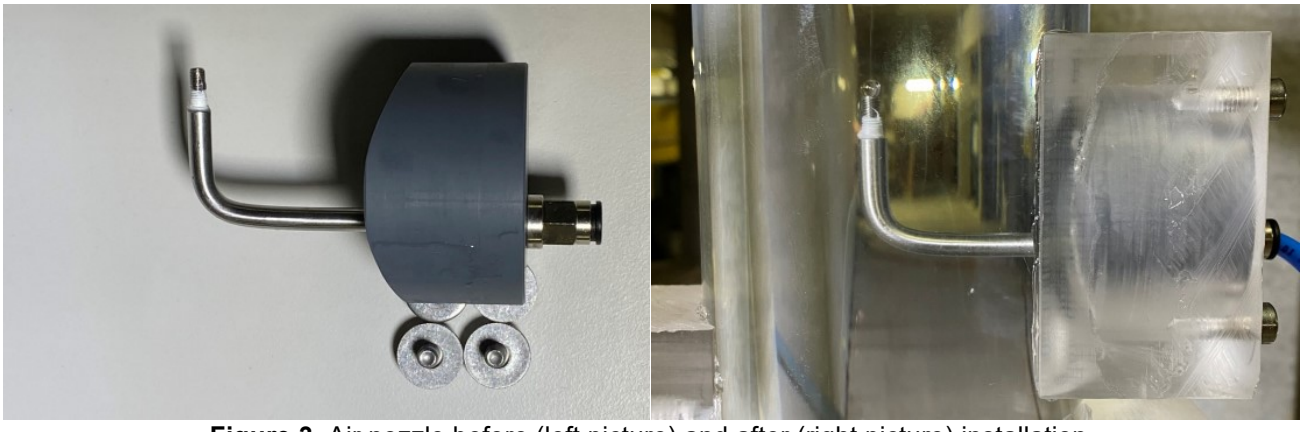

Figure 3. Air nozzle before (left picture) and after (right picture) installation.

2.3 Stereo-view Setup

The camera used to record bubble-probe interactions was a FASTCAM Mini AX50 type 170K-M-8GB, characterized by a maximum frame rate of 170,000 fps at a resolution of 128 x 16 pixels, trigger inputs, 12-bit monochrome Dynamic Range and 8GB of internal memory. For this experimental campaign, the camera was used at a framerate of 20,000 fps and a resolution of 256 x 256 pixels, allowing a maximum recording duration of 4.28 sec, i.e., 85,600 frames. To get an accurate estimation of the velocity of the bubbles and to perform a 3D reconstruction of their shape, a simultaneous recording from different perspectives was needed. This was achieved by using a single camera and a custom-made beam splitter, which allows perfect synchronization of a stereoscopic view but comes at the cost of decreased image resolution.

The base of the beam splitter consisted of a PVC table characterized by five engravings obtained by 0.5 mm precise CNC milling; these were used to precisely arrange the mirror components, together with the help of adjustable clamping arms (Fig. 4b). The components included a knife-edge right-angle prism coated with aluminum mirror, two uncoated right-angle prisms and two right-angle prism mirrors coated with aluminum (Fig. 4a). All the prisms were characterized by a side dimension of L = 25 mm and a reflection light wavelength ranging from 450 nm to 20 µm. Both the camera and the stereo-view system were mounted on a tailor-made frame composed of stiff aluminum bars connected to the concrete ceiling, to avoid vibrations during the tests while still allowing free adjustments along all three directions. In addition, both the camera and the beam splitter table were mounted to the aluminum frame using tripod heads with micrometric knobs and inbuilt levelling bubbles which allowed more precise adjustments.

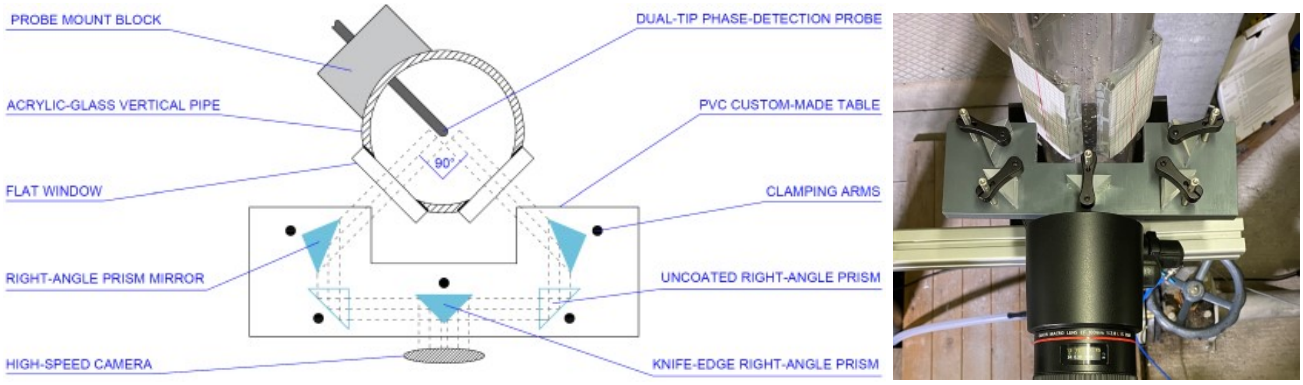

Figure 4. Sketch and picture of the beam splitter setup. The paper markings on the two windows were used for a first rough alignment of beam splitter and camera.

3. METHODOLOGY

A total of 30 tests were performed, and three values of vertical water velocity were investigated: V_w = 0.0, 0.5 and 1.0 m/s. Table 1 lists the main hydraulic parameters characterizing the experimental tests conducted. During each test, the gate valve was operated until the target value of water discharge Q_w was reached. At that point, the air pressure reduction valve was set to 0.5 bar, and the butterfly air valve was slowly opened until the air bubbles were starting to be injected into the vertical acrylic-glass pipe. The pressure sensor displayed the value of air pressure P_a injected into the rising water flow. Then, the recording of the dual-tip phase-detection probe signal was started. The first bubble hitting the leading tip sent a trigger signal to the high-speed camera which then saved the frames before and after the trigger release (centered trigger). The procedure was then repeated to create 10 tests with complete dual-tip phase-detection probe recordings (i.e., the bubble hitting both tips) for each value of water velocity.

For this study, the probe data were registered using LabVIEW, while the high-speed camera was operated by the Photron Fastcam Viewer 4 (PFV4) software. Data were then processed and analyzed independently, and qualitative and quantitative comparisons were made.

Table 1. List of the experimental tests

Test n.	V_w [m/s]	Q_w [l/s]	P_a [bar]
1	0.00	0.00	0.109
2	0.50	3.18	0.105
3	1.00	6.36	0.107

©2022 IAHR. Used with permission / ISSN-L 2521-7119

3.1 Phase-Detection Probe Data Processing

For each test, the probe recorded at a frequency f_p = 2,000 KHz for 5 s. Three channels were recorded, i.e., the raw S_{1r} and digital S_{1d} signals of the leading tip and the raw S_{2r} signal of the trailing tip (Fig. 5). The signals were then post-processed by using the MATLAB (2021) Signal Processing Toolbox. The digital signal of the leading tip was used as a trigger for the video recording, releasing a trigger as soon as the voltage dropped below 2.5 V. In the probe signal, a high value of voltage corresponds to water surrounding the probe tips, while values close to zero are associated to air (see Fig. 5). The raw signals were used to estimate the bubble velocity V_p and the chord times $(t_{c1})_p$ and $(t_{c2})_p$, i.e., the amount of time that the leading and trailing probe tips spent inside the bubble, respectively. To do so, the indices i_1, i_2, i_3 and i_4 were estimated, corresponding to the instants when the leading and trailing tips entered and left the bubble, i.e., t_1, t_2, t_3, t_4, respectively. These were determined using a single voltage threshold of 4 V, corresponding to common practice in bubbly flows (e.g., Revankar & Ishii, 1992; Kim et al., 2000). To this end, Fig. 5a and b show the threshold level used to determine t_1, t_2, t_3, t_4 for the raw signals of the leading and trailing tip, respectively. Afterwards, the parameters of interest were estimated as $V_p = \Delta y/(t_3 - t_1)$, $(t_{c1})_p = t_2 - t_1$ and $(t_{c2})_p = t_4 - t_3$. Due to the nature of the tests, i.e., single bubbles interacting with the probe, the analysis did not follow the typically used method in hydraulic engineering for highly-aerated flows, where the most probable travel times of the gas–liquid interfaces are estimated by performing a cross-correlation analysis over groups of multiple bubbles (Kramer et al. 2020).

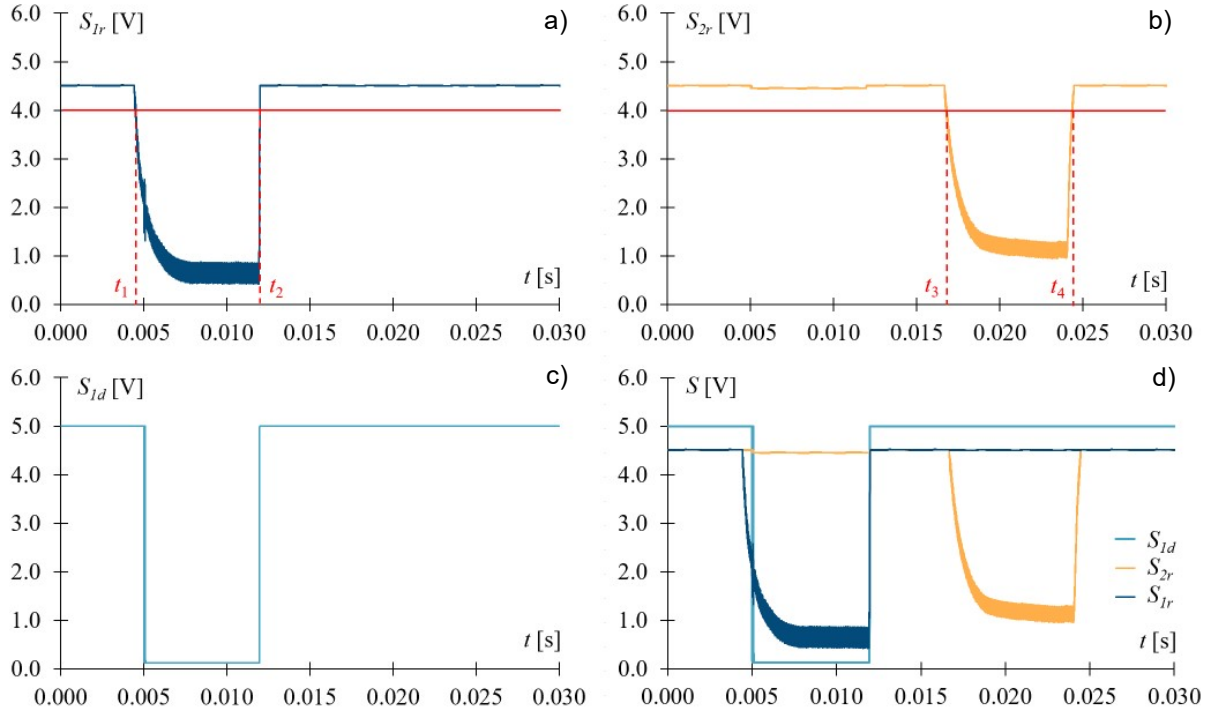

Figure 5. Raw signal of the a) leading and b) trailing tip, including the 4 V threshold to determine t_1, t_2, t_3, t_4; c) digital signal of the leading tip; d) combined data.

3.2 High-Speed Camera Data Processing

For each tested condition, videos of the bubble-probe interaction were recorded, and the resulting files were post-processed by using the MATLAB (2021) Computer Vision Toolbox. The capturing process started when a bubble pulled the digital trigger by hitting the leading tip of the probe; at this point, a recording window ≈ 1 s long centered on the trigger-pulling frame was automatically saved, and it was then manually cropped to durations smaller than 0.05 seconds for an easier handling of the resulting raw file format. All the tests were recorded with the following high-speed camera settings: framerate, f_c = 20,000 fps, shutter speed of 1/950,000 sec, resolution of 256x256 pixels. In addition, the post-processing operations are schematically presented in Figure 6. First, for each test, all frames were extracted from the video recordings and stored locally. Then, each frame was divided into a left and a right part, i.e., view from the left and right mirrors of the beam splitter (step 1), and each portion was analyzed independently. The mean intensity of each pixel throughout all the frames was subtracted from each pixel, to remove the background from the picture (step 2), then image binarization was performed (step 3). Finally, for each frame, an ellipse defined by the centroid $O = (x_O; y_O)$, the major axis a, the minor axis b, and the orientation θ was fitted to the x-y and z-y projections of the bubble (step 4). Note

that in the text the subscripts “dx” and “sx” refer to the right and left portion of the view from the beam splitter, respectively.

The parameters defining the ellipses fitted at each frame led to the estimation of important quantities characterizing air bubbles, schematically presented in Figure 7. First, the frame-by-frame instantaneous bubble velocities were computed by applying the finite differences method to the ellipse centroid *O*. For both the left and right images, the vertical and horizontal velocity components were estimated, i.e., V_x, $(V_y)_{sx}$, V_z, $(V_y)_{dx}$, respectively. It is worth mentioning that for the reference system chosen and for the geometrical characteristics of the setup, $(V_y)_{sx} \approx (V_y)_{dx} \equiv V_y$. Furthermore, the magnitude of the bubble centroid velocity in space was estimated as $|V| = (V_x^2 + V_y^2 + V_z^2)^{1/2}$. Then, for each frame, a 3D reconstruction of the bubble was performed by assuming an ellipsoid of axes $j = a_{sx}$, $k = a_{dx}$ and $l = 0.5\,(b_{sx} + b_{dx})$; the volume of the ellipsoid was computed and, at each frame, the equivalent bubble diameter d_{eq} was estimated. Last, the chord time $(t_{c1})_c$ was calculated by counting the frames for which the leading tip was lying simultaneously inside the x-y and z-y bubble projections; in the same fashion, $(t_{c2})_c$ was estimated for the trailing tip. Thereafter, by knowing the frames corresponding to the bubble entering and leaving each of the probe tips, four different estimations of the velocity along the y-axis were distinguished, i.e., $|V_{cy}|_{BI}$, $|V_{cy}|_{DI}$, $|V_{cy}|_{AI}$, $|V_{cy}|_G$, corresponding to the modulus of the vertical velocity component before (subscript “BI”), during (subscript “DI”) and after (subscript “AI”) the interaction with the probe tips and to the global (subscript “G”) value of $|V_{cy}|$ averaged over all the frames available. It is worth mentioning that we always refer to the absolute value of the vertical component of the bubble centroid velocity since its value is always negative according to the reference system adopted (Fig. 7).

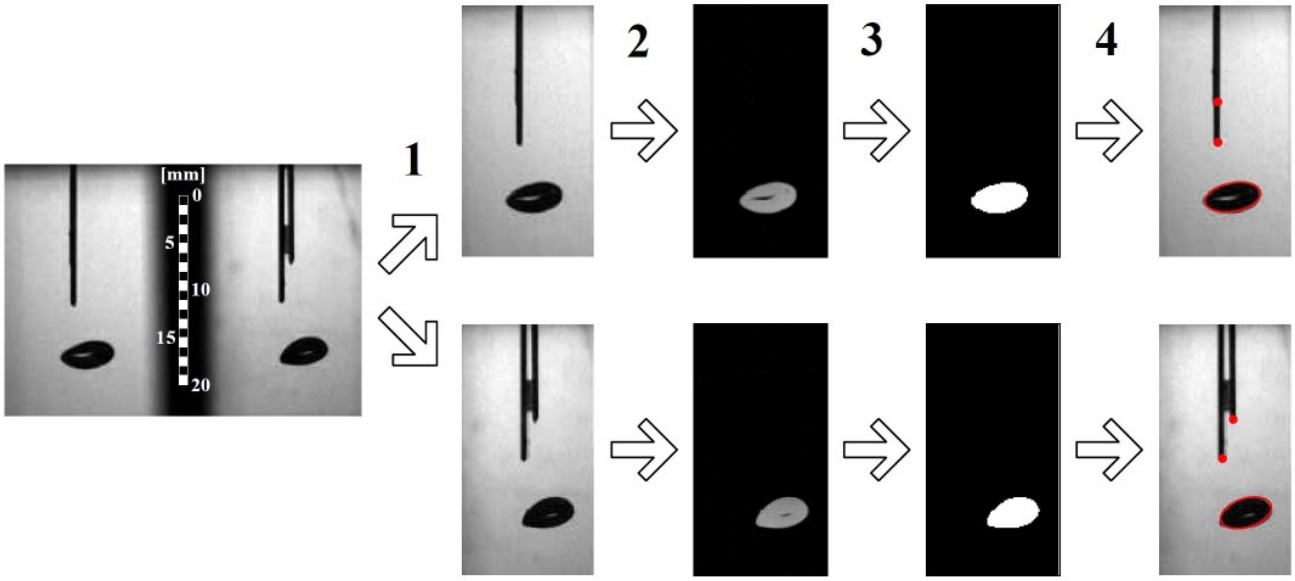

Figure 6. Steps for the post-processing of the frames extracted from the high-speed camera recordings. In the first picture to the left, the scale bar suggests the real dimension of the elements depicted.

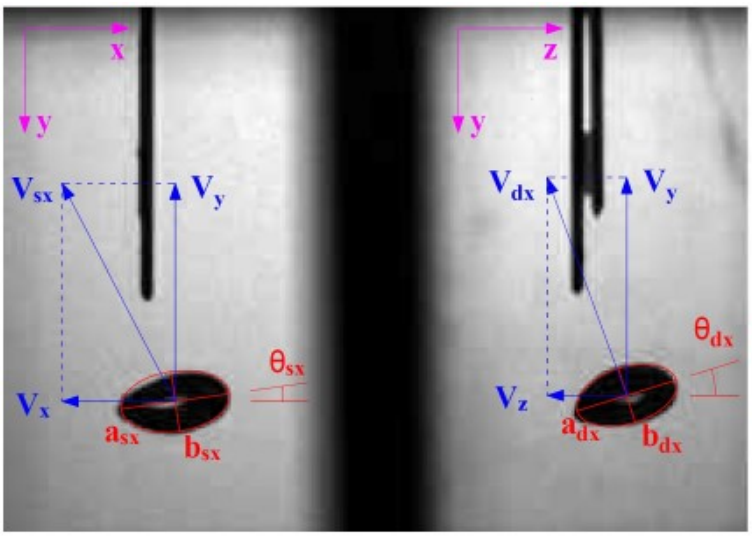

Figure 7. Reference system adopted.

©2022 IAHR. Used with permission / ISSN-L 2521-7119

4. RESULTS AND DISCUSSION

The data obtained from the experimental tests were analyzed and compared for the validation of the dual-tip phase-detection probe. First, the bubble velocities measured by the probe V_p were compared to the y-component estimated from the high-speed camera during the bubble-probe interaction, i.e., $|V_{cy}|_{DI}$ (Fig. 8a). The plot shows a good agreement between the two datasets, suggesting a slight tendency of the velocities estimated from the high-speed camera to be smaller than the ones measured by the probe. In addition, Figure 8b shows that the relative percentage difference between the two estimations is higher for $|V_{cy}|_{DI} < 0.5$ m/s than for larger velocities, and that the probe tends to overestimate in this region. As $|V_{cy}|_{DI}$ increases, no systematic trend can be observed, with most of the observations lying inside a ±20% interval. This discrepancy is mainly due to the geometry of the bubbles involved, since ideally the probe measurements would match the real counterparts only for a flat bubble interface impacting the needles perpendicularly (see Leung et al., 1995; Mishra et al., 2002). While these effects tend to average out over many bubbles since the impact location and angle are symmetrically distributed, they can lead to significant deviations when investigating single bubbles. In addition, smaller uncertainties are introduced by the wetting and drying processes of the probe tips, affecting the estimation of the indices i_1, i_2, i_3, i_4, and in turn influencing the value of V_p (Luther, 2004; Kramer et al., 2020b).

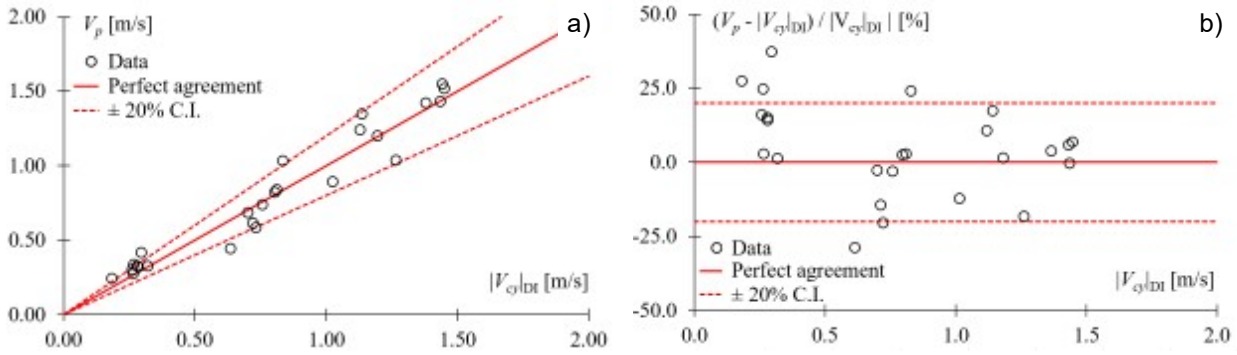

Figure 8. a) V_p and b) $(V_p - |V_{cy}|_{DI})/|V_{cy}|_{DI}$ vs. $|V_{cy}|_{DI}$, measured during the bubble-probe interaction.

From the video recordings, a deflection, deformation and slowing down of the bubbles after interacting with the probe can be often noticed similar to mechanisms described in Hohermuth et al. (2021). To assess bubble deceleration, the ratio of $|V_{cy}|$ computed before and during the bubble probe interaction (i.e., $|V_{cy}|_{BI}/|V_{cy}|_{DI}$) was plotted against the global value (i.e., $|V_{cy}|_G$), grouped by different equivalent diameter ranges, i.e., $2.5 \le d_1 < 4.0$ mm; $4.0 \le d_2 < 4.5$ mm; $4.5 \le d_3 < 5.0$ mm; $5.0 \le d_4 < 5.5$ mm; $5.5 \le d_5 < 6.5$ mm (see Figure 9). The effect seems to particularly influence bubbles travelling at velocities $|V_{cy}|_G < 0.5$ m/s, while for larger velocities the effect tends to decrease in agreement with the theory of Hohermuth et al. (2021).

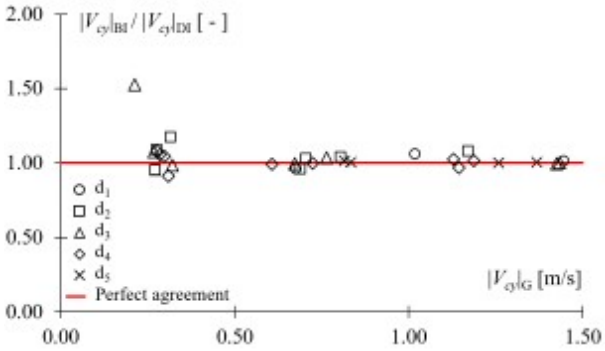

Figure 9. $|V_{cy}|_{BI}/|V_{cy}|_{DI}$ vs. $|V_{cy}|_G$, together with the perfect agreement line.

Finally, Figure 10 shows a comparison of the chord times $(t_{c1})_c$, $(t_{c2})_c$, $(t_{c1})_p$, $(t_{c2})_p$ estimated from camera recordings and probe for the leading and the trailing tip, respectively. Figure 10a shows a good agreement between $(t_{c1})_c$ and $(t_{c1})_p$, suggesting that the chord times estimated from the high-speed camera tend to be slightly larger than the probe counterpart for smaller velocities. When comparing the data from the trailing tip, results appear to be more scattered (Figure 10b), confirming that the most reliable estimation of the chord time is given by the leading tip, due to piercing, deformation, and crawling effects on the bubble during the interaction (Hohermuth et al., 2021). To strengthen this statement, when comparing the chord times of the leading tip

versus trailing tip from the same estimation method, data seem to be more scattered than the ones shown by the analogous comparison of the leading tip estimations (Figures 10c, d).

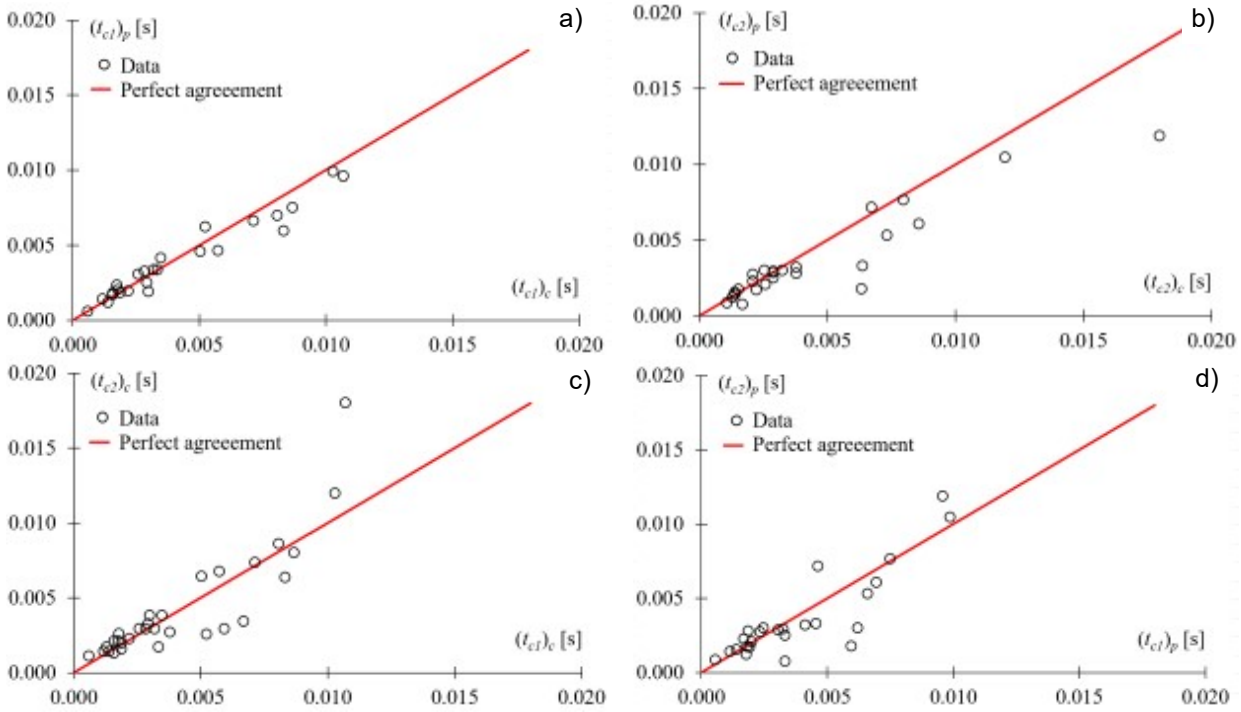

Figure 10. Chord times comparison: a) leading tip and b) trailing tip (camera vs probe); leading vs trailing tip for c) camera and d) probe.

5. CONCLUSIONS

A custom-made experimental setup was built in the Laboratory of Hydraulics, Hydrology and Glaciology (VAW), ETH Zurich, to validate a dual-tip phase-detection conductivity probe against a high-speed camera. Bubbles were inserted via an air nozzle into an acrylic-glass vertical pipe with upwards-flowing water at velocities $0 \leq V_w \leq 1$ m/s, resulting in air bubbles of equivalent diameter ranging between $2.5 \leq d_{eq} \leq 6.5$ mm. The main parameters characterizing air-water flows, i.e., bubble velocity V, leading tip chord time t_{c1}, trailing tip chord time t_{c2}, were measured by means of a dual-tip conductivity probe and of a stereo-view optical system, made up of a high-speed camera and a beam splitter. Results showed a good agreement between the velocities estimated with the probe and the vertical component of the velocities estimated by the optical method, with some biases for bubble velocities smaller than 0.5 m/s, where the probe tends to overestimate bubble velocities. In general, within the tested range of velocities, most of the conductivity probe measurements lie inside the ±20% of the camera-based velocity. Indeed, the discrepancies are partially due to uncertainties introduced by wetting and drying processes of the probe tips and to the assumptions behind probe estimations (i.e., flat bubble surface and perpendicular bubble-probe interaction), as well as by crawling effects, influencing the probe velocity estimations. Regarding the chord times, a good agreement is shown for the leading tip between the two methods, i.e., $(t_{c1})_c$ and $(t_{c1})_p$, while greater inaccuracies appear when the trailing tip counterparts, i.e., $(t_{c2})_c$ and $(t_{c2})_p$, are involved, due to the crawling effect influencing bubble shape, direction and velocity. However, the exact mechanisms occurring during bubble-probe interactions and the uncertainties in both the measurement methods need to be analyzed in more detail.

6. ACKNOWLEDGEMENTS

The authors thank Prof. Dr. Outi Supponen and Guillaume Bokman from the Institute of Fluid Dynamics, ETH Zurich, for letting us use their high-speed camera and helping us with the setup. The support of the technical staff of the Laboratory of Hydraulics, Hydrology and Glaciology (VAW), ETH Zurich is gratefully acknowledged; Patrick Egli, Stefan Gribi, Daniel Gubser, Raphael Heini, Dorde Masovic, Mario Moser, Andreas Schlumpf, Henry Zoller (in alphabetical order). The project is supported by the Swiss National Science Foundation (SNSF, Grant 200020_197208).

©2022 IAHR. Used with permission / ISSN-L 2521-7119

7. REFERENCES

Barre, S., Rolland, J., Boitel, G., Goncalves, E., & Patella, R. F. (2009). Experiments and modeling of cavitating flows in venturi: attached sheet cavitation. *European Journal of Mechanics-B/Fluids*, *28*(3), 444-464.

Boes, R. M., & Hager, W. H. (2003). Hydraulic design of stepped spillways. *Journal of Hydraulic Engineering*, *129*(9), 671-679.

Cartellier, A., & Achard, J. L. (1991). Local phase detection probes in fluid/fluid two-phase flows. *Review of Scientific Instruments*, *62*(2), 279-303.

Chanson, H. (2007). Bubbly flow structure in hydraulic jump. *European Journal of Mechanics-B/Fluids*, *26*(3), 367-384.

Chanson, H. (2013). Hydraulics of aerated flows: qui pro quo?. *Journal of Hydraulic Research*, *51*(3), 223-243.

Chanson, H., & Toombes, L. (2002). Air–water flows down stepped chutes: turbulence and flow structure observations. *International Journal of Multiphase Flow*, *28*(11), 1737-1761.

Felder, S., & Chanson, H. (2014). Triple decomposition technique in air–water flows: application to instationary flows on a stepped spillway. *International Journal of Multiphase Flow*, *58*, 139-153.

Felder, S., & Chanson, H. (2017). Scale effects in microscopic air-water flow properties in high-velocity free-surface flows. *Experimental Thermal and Fluid Science*, *83*, 19-36.

Felder, S., & Pfister, M. (2017). Comparative analyses of phase-detective intrusive probes in high-velocity air–water flows. *International Journal of Multiphase Flow*, *90*, 88-101.

Felder, S., & Severi, A. (2016, December). Entrapped air in high-velocity free-surface flows on a flat-sloped spillway. In *Proceedings of 20th Australasian Fluid Mechanics Conference*, Perth, WA.

Felder, S., Hohermuth, B., & Boes, R. M. (2019). High-velocity air-water flows downstream of sluice gates including selection of optimum phase-detection probe. *International Journal of Multiphase Flow*, *116*, 203-220.

Hibiki, T., Hogsett, S., & Ishii, M. (1998). Local measurement of interfacial area, interfacial velocity and liquid turbulence in two-phase flow. *Nuclear engineering and design*, *184*(2-3), 287-304.

Hohermuth, B., Kramer, M., Felder, S., & Valero, D. (2021). Velocity bias in intrusive gas-liquid flow measurements. *Nature communications*, *12*(1), 1-9.

Ishii, M., & Kim, S. (2001). Micro four-sensor probe measurement of interfacial area transport for bubbly flow in round pipes. *Nuclear engineering and design*, *205*(1-2), 123-131.

Kaichiro, M., & Ishii, M. (1984). Flow regime transition criteria for upward two-phase flow in vertical tubes. *International Journal of Heat and Mass Transfer*, *27*(5), 723-737.

Kim, S., Fu, X. Y., Wang, X., & Ishii, M. (2000). Development of the miniaturized four-sensor conductivity probe and the signal processing scheme. *International journal of heat and mass transfer*, *43*(22), 4101-4118.

Kramer, K., & Hager, W. H. (2005). Air transport in chute flows. *International Journal of Multiphase Flow*, *31*(10-11), 1181-1197.

Kramer, M., & Chanson, H. (2019). Optical flow estimations in aerated spillway flows: Filtering and discussion on sampling parameters. *Experimental Thermal and Fluid Science*, *103*, 318-328.

Kramer, M., Chanson, H., & Felder, S. (2020a). Can we improve the non-intrusive characterization of high-velocity air–water flows? Application of LIDAR technology to stepped spillways. Journal of Hydraulic Research, 58(2), 350-362.

Kramer, M., Hohermuth, B., Valero, D., & Felder, S. (2020b). Best practices for velocity estimations in highly aerated flows with dual-tip phase-detection probes. *International Journal of Multiphase Flow*, *126*, 103228.

Leung, W. H., Revankar, S. T., Ishii, Y., & Ishii, M. (1995). Axial development of interfacial area and void concentration profiles measured by double-sensor probe method. *International journal of heat and mass transfer*, *38*(3), 445-453.

Lucas, G., Zhao, X., & Pradhan, S. (2011). Optimisation of four-sensor probes for measuring bubble velocity components in bubbly air–water and oil–water flows. *Flow Measurement and Instrumentation*, *22*(1), 50-63.

Luther, S., Rensen, J., & Guet, S. (2004). Bubble aspect ratio and velocity measurement using a four-point fiber-optical probe. *Experiments in fluids*, 36(2), 326-333.

MATLAB. (2021). version 9.11.0 (R2021b). Natick, Massachusetts: The MathWorks Inc.

Mishra, R., Lucas, G. P., & Kieckhoefer, H. (2002). A model for obtaining the velocity vectors of spherical droplets in multiphase flows from measurements using an orthogonal four-sensor probe. *Measurement Science and Technology*, *13*(9), 1488.

Neto, I. E. L., Zhu, D. Z., & Rajaratnam, N. (2008). Bubbly jets in stagnant water. *International Journal of Multiphase Flow*, *34*(12), 1130-1141.

Nguyen, V. T., & Bui, H. (2019). Development of Conductivity Probe and Signal Processing Algorithm for Measuring of Local Two-Phase Flow Parameters.

Perret, M. N. (2016). Local optical phase detection probes with an application to a high-speed boundary layer. *PhD Thesis*, University of Iowa.

Pfister, M., Hager, W. H., & Boes, R. M. (2014). Trajectories and air flow features of ski jump-generated jets. *Journal of Hydraulic Research*, *52*(3), 336-346.

Revankar, S. T., & Ishii, M. (1992). Local interfacial area measurement in bubbly flow. *International journal of heat and mass transfer*, *35*(4), 913-925.

Shen, X., Hibiki, T., & Nakamura, H. (2012). Developing structure of two-phase flow in a large diameter pipe at low liquid flow rate. *International journal of heat and fluid flow*, *34*, 70-84.

Shen, X., Saito, Y., Mishima, K., & Nakamura, H. (2005). Methodological improvement of an intrusive four-sensor probe for the multi-dimensional two-phase flow measurement. *International journal of multiphase flow*, *31*(5), 593-617.

Shen, X., Saito, Y., Mishima, K., & Nakamura, H. (2006). A study on the characteristics of upward air–water two-phase flow in a large diameter pipe. *Experimental thermal and fluid science*, *31*(1), 21-36.

Takahashi, M., & Ohtsu, I. (2012). Aerated flow characteristics of skimming flow over stepped chutes. *Journal of Hydraulic Research*, *50*(4), 427-434.

Tian, D., Yan, C., & Sun, L. (2015). Model of bubble velocity vector measurement in upward and downward bubbly two-phase flows using a four-sensor optical probe. *Progress in nuclear energy*, *78*, 110-120.

Toombes, L., & Chanson, H. (2008). Interfacial aeration and bubble count rate distributions in a supercritical flow past a backward-facing step. *International Journal of Multiphase Flow*, *34*(5), 427-436.

Vejražka, J., Večeř, M., Orvalho, S., Sechet, P., Ruzicka, M. C., & Cartellier, A. (2010). Measurement accuracy of a mono-fiber optical probe in a bubbly flow. *International Journal of Multiphase Flow*, *36(7)*, 533-548.

Wang, K., Tang, R., Bai, R., & Wang, H. (2021). Evaluating phase-detection-based approaches for interfacial velocity and turbulence intensity estimation in a highly-aerated hydraulic jump. *Flow Measurement and Instrumentation*, *81*, 102045.

Wongwailikhit, K., Dietrich, N., Hébrard, G., & Painmanakul, P. (2019). Performance of a monofiber optical probe in determining the droplet size and velocity in spray systems compared with a high-speed camera. *Industrial & Engineering Chemistry Research*, *58*(51), 23366-23379.

Xing, D., Yan, C., Ma, X., & Sun, L. (2014). Effects of void fraction correlations on pressure gradient separation of air–water two-phase flow in vertical mini rectangular ducts. *Progress in Nuclear Energy*, *70*, 84-90.

©2022 IAHR. Used with permission / ISSN-L 2521-7119